

# On an origami structure of period-1 motions to homoclinic orbits in the Rössler system

Cite as: Chaos **32**, 123121 (2022); <https://doi.org/10.1063/5.0131970>

Submitted: 25 October 2022 • Accepted: 15 November 2022 • Published Online: 09 December 2022

 Siyuan Xing and  Albert C. J. Luo

## COLLECTIONS

Paper published as part of the special topic on [Constructed complex motions and chaos](#)



[View Online](#)



[Export Citation](#)



[CrossMark](#)

## ARTICLES YOU MAY BE INTERESTED IN

### [Review of sample-based methods used in an analysis of multistable dynamical systems](#)

Chaos: An Interdisciplinary Journal of Nonlinear Science **32**, 082101 (2022); <https://doi.org/10.1063/5.0088379>

### [Quantifying chaos using Lagrangian descriptors](#)

Chaos: An Interdisciplinary Journal of Nonlinear Science **32**, 123122 (2022); <https://doi.org/10.1063/5.0120889>

### [Equilibrium and symmetries of altitudinal magnetic rotors on a circle](#)

Chaos: An Interdisciplinary Journal of Nonlinear Science **32**, 123120 (2022); <https://doi.org/10.1063/5.0119916>



**Chaos**  
Special Topic: Nonlinear Model Reduction From Equations and Data  
**Submit Today!**

The banner features a blue-to-red gradient background with a digital, geometric pattern of binary code and mathematical symbols on the left side.

# On an origami structure of period-1 motions to homoclinic orbits in the Rössler system

Cite as: Chaos 32, 123121 (2022); doi: 10.1063/5.0131970

Submitted: 25 October 2022 · Accepted: 15 November 2022 ·

Published Online: 9 December 2022



Siyuan Xing<sup>1,a)</sup> and Albert C. J. Luo<sup>2,b)</sup>

## AFFILIATIONS

<sup>1</sup>Department of Mechanical Engineering, California Polytechnic State University, San Luis Obispo, California 93407, USA

<sup>2</sup>Department of Mechanical and Mechatronics Engineering, Southern Illinois University Edwardsville, Edwardsville, Illinois 62026-1805, USA

**Note:** This paper is part of the Focus Issue on Constructed complex motions and chaos.

**a) Author to whom correspondence should be addressed:** [sixing@calpoly.edu](mailto:sixing@calpoly.edu)

**b)** [aluo@siue.edu](mailto:aluo@siue.edu)

## ABSTRACT

In this paper, an origami structure of period-1 motions to spiral homoclinic orbits in parameter space is presented for the Rössler system. The edge folds of the origami structure are generated by the saddle-node bifurcations. For each edge, there are two layers to form the origami structure. On one layer of the origami structure, there is a pair of period-doubling bifurcations inducing periodic motions from period-1 to period- $2^n$  motions ( $n = 1, 2, \dots, \infty$ ). On such a layer, the unstable period-1 motion goes to the homoclinic orbits with a mapping eigenvalue approaching negative infinity. However, on the corresponding adjacent layers, no period-doubling bifurcations exist, and the unstable period-1 motion goes to the homoclinic orbit with a mapping eigenvalue approaching positive infinity. To determine the origami structure of the period-1 motions to homoclinic orbits, the implicit map of the Rössler system is developed through the discretization of the corresponding differential equations. The Poincaré mapping section can be selected arbitrarily. Before construction of the origami structure, the bifurcation diagram of periodic motions varying with one parameter is developed, and trajectories of stable periodic motions on the bifurcation diagram to homoclinic orbits are illustrated. Finally, the origami structures of period-1 motions to homoclinic orbits are developed through a few layers. This study provides the mathematical mechanisms of period-1 motions to homoclinic orbits, which help one better understand the complexity of periodic motions near the corresponding homoclinic orbit. There are two types of infinitely many homoclinic orbits in the Rössler system, and the corresponding mapping structures of the homoclinic orbits possess positive and negative infinity large eigenvalues. Such infinitely many homoclinic orbits are induced through unstable periodic motions with positive and negative eigenvalues accordingly.

Published under an exclusive license by AIP Publishing. <https://doi.org/10.1063/5.0131970>

A full understanding of dynamics for periodic orbits to homoclinic orbits is very significant to determine motion singularity and complexity in nonlinear dynamical systems. Since 1960, one tried to qualitatively and quantitatively study the mathematical structures of periodic orbits near homoclinic orbits in three-dimensional nonlinear systems (e.g., the Lorenz system and the Rössler system). In the past six decades, indeed, one has a better understanding of homoclinic orbit formation in such systems based on the linearized approximate theory and numerical studies, but such a problem to be solved is still far away. Thus, the mathematical structure of periodic motions to homoclinic orbits should be further studied. In this paper, the origami structure of period-1 motions to spiral homoclinic orbits is developed semi-analytically through an implicit mapping method. The origami structure with infinite layers in parameter space guides periodic

motions to homoclinic orbits with one of eigenvalues going to positive and negative infinity. The quasi-homoclinic orbits (periodic) near the homoclinic orbits on each layer of the origami structure are illustrated for better demonstrations of possible homoclinic orbits.

## I. INTRODUCTION

As proposed by Rössler,<sup>1,2</sup> consider the Rössler system as

$$\begin{aligned}\dot{x} &= -(y + z), \\ \dot{y} &= x + ay, \\ \dot{z} &= b + z(x - c).\end{aligned}\tag{1}$$

The system parameters are  $a, b, c$ . If  $c^2 - 4ab > 0$ , the foregoing system has two equilibria,

$$\mathbf{x}_\pm^* = (ap_\pm, p_\pm, p_\pm)^T \text{ with } p_\pm = \frac{-c \pm \sqrt{c^2 - 4ab}}{2a}. \quad (2)$$

The equilibrium  $\mathbf{x}_+^*$  is a saddle. For  $c^2 = 4ab$ , the two equilibria merge a critical equilibrium. For  $c^2 < 4ab$ , the Rössler system does not have any equilibria. Such a system has a quadratic nonlinear term with six linear terms, which is one of the simplest three-dimensional nonlinear systems. However, the Lorenz system<sup>3</sup> has two nonlinear terms plus five linear terms, and chaotic motions were demonstrated. Near a homoclinic orbit, a denumerable set of periodic motions exists, which was proved by Shilnikov.<sup>4,5</sup> In 1972, Gavrilov and Shilnikov<sup>6</sup> studied a structurally unstable homoclinic orbit in three-dimensional dynamical systems, which was based on the local eigenvalue analysis. In 1973, Gavrilov and Shilnikov<sup>7</sup> studied dynamical systems with a structurally unstable homoclinic curve. Recently, one found that the Lorenz system has complex periodic motions near the homoclinic orbits and the possible infinite homoclinic orbits exist.<sup>8–11</sup> Thus, one asked whether the Rössler system has complex periodic motion near the homoclinic orbits like the Lorenz system or not. To answer such a question is one of the authors' purposes in this paper. Thus, the Rössler system will be studied, and the origami structure of periodic motions to homoclinic orbits will be developed for a global view of relationship from periodic motions to homoclinic orbits.

Since 1976, one has tried to dig out the dynamical behaviors of the Rössler system. In 1982, from the Shilnikov theorem, Arneodo *et al.*<sup>12</sup> illustrated chaotic behaviors of the Rössler system, and there might exist infinitely many unstable periodic orbits of saddle-type. In 1984, Glendinning and Sparrow<sup>13</sup> discussed the local and global behaviors of periodic orbits near homoclinic orbits through the two-dimensional maps, and such maps were constructed from the corresponding linearized system and an assumed circular function for the proposed spiral motion, which are based on numerical observations. At the same time, Gaspard *et al.*<sup>14</sup> used the similar ideas to construct the two-dimensional map to determine the bifurcation phenomena near homoclinic orbits in bi-parameter space, and the spiral periodic orbits of the Rössler system were discussed. Such analysis mainly originated from the Shilnikov local analysis. In 1985, Gardini<sup>15</sup> discussed Hopf bifurcations and period-doubling transitions in the Rössler system through the local eigenvalue analysis of equilibrium and numerically demonstrated chaotic attractors in the Rössler system. Arneodo *et al.*<sup>16</sup> completed the local analysis to achieve truncated normal forms of nonlinear systems and used the similar method to construct the similar two-dimensional map for reduction to the unidimensional map with a limit case. Through such analysis based on the two-dimensional maps, one still cannot obtain a global picture of periodic orbits near the homoclinic orbits. Thus, in 1994, numerical detection and continuation of co-dimensional-two homoclinic bifurcations were developed in Champneys and Kuznetsov.<sup>17</sup> Such a method is based on the eigenvectors at the hyperbolic equilibrium with the integration constraint and the homotopy to construct an approximate homoclinic orbit. In 1995, Letellier *et al.*<sup>18</sup> considered a Poincaré section at the equilibrium of  $x = x_-^*$  with positive crossings by increasing x-coordinates

for the Rössler system. Through such a section, one tried to find the first-return maps to determine unstable periodic motions numerically. Further studies of the Rössler system were reported (e.g., Refs. 19–22). Those studies were based on the Poincaré section with the first-return map and AUTO to determine the periodic motion near the homoclinic orbits.

In the afore-mentioned studies, the Poincaré section should be carefully selected for the first-return map, and the used numerical simulations cannot obtain unstable periodic motions in three-dimensional nonlinear systems, such as Rössler and Lorenz systems. In 2015, Luo<sup>23,24</sup> developed an implicit mapping method for stable and unstable periodic motions in nonlinear dynamical systems. Luo and Guo<sup>25</sup> used such an implicit mapping method for periodic motions in a periodically forced Duffing oscillator. The semi-analytical results were compared with the analytical solutions of periodic motions in Luo and Huang.<sup>26</sup> To determine unstable and stable periodic motions in the Rössler system, the implicit mapping method will be used in this paper. Through such an implicit method, the Poincaré mapping can be selected arbitrarily. The implicit mapping will be developed through the discretization of differential equations. From a mapping structure, periodic motions will be determined with a starting section as a Poincaré section. The stability and bifurcations of periodic motions will be determined through the corresponding eigenvalue analysis. From the eigenvalue constraints of  $\lambda = 1$  and  $\lambda = -1$ , the boundary curves varying with parameters will be determined for saddle-node and period-doubling bifurcations. Thus, an origami structure of periodic motions to homoclinic orbits will be developed in the bi-parameter space.

## II. EQUILIBRIUM STABILITY AND BIFURCATION

Consider the Rössler system as

$$\dot{\mathbf{x}} = \mathbf{f}(\mathbf{x}, \mathbf{p}), \quad (3)$$

where

$$\mathbf{x} = (x_1, x_2, x_3)^T, \mathbf{f} = (f_1, f_2, f_3)^T, \mathbf{p} = (a, b, c)^T \quad (4)$$

and

$$\begin{aligned} f_1 &= -(y + z), \\ f_2 &= x + ay, \\ f_3 &= b + z(x - c). \end{aligned} \quad (5)$$

At the equilibrium  $\mathbf{x}_\pm^*$ , the variational equation is

$$\Delta \dot{\mathbf{x}} = D\mathbf{f}(\mathbf{x}_\pm^*, \mathbf{p}) \Delta \mathbf{x}, \quad (6)$$

and the Jacobian matrix is

$$D\mathbf{f}(\mathbf{x}_\pm^*, \mathbf{p}) = \begin{bmatrix} 0 & -1 & -1 \\ 1 & a & 0 \\ z_\pm^* & 0 & (x_\pm^* - c) \end{bmatrix}. \quad (7)$$

The stability and bifurcations of the equilibrium are determined by eigenvalues of the Jacobian matrix; i.e.,

$$|D\mathbf{f}(\mathbf{x}_\pm^*, \mathbf{p}) - \lambda \mathbf{I}| = \begin{vmatrix} -\lambda & -1 & -1 \\ 1 & a - \lambda & 0 \\ z_\pm^* & 0 & (x_\pm^* - c) - \lambda \end{vmatrix} = 0. \quad (8)$$

With varying system parameters, the Rössler system has three cases for the equilibriums.

- (i) If  $c^2 < 4ab$ , no equilibriums exist in the Rössler system.
- (ii) For  $c^2 = 4ab$ , there is one equilibrium given by

$$\mathbf{x}_\pm^* = \left( -\frac{c}{2}, -\frac{c}{2a}, -\frac{c}{2a} \right)^T. \quad (9)$$

- (iii) For  $c^2 > 4ab$ , there are two equilibriums as in Eq. (2). If the parameters  $a$  and  $b$  are finite, for  $c \rightarrow \pm\infty$ , the two equilibriums are

$$\left. \begin{aligned} \mathbf{x}_-^* &\approx \left( -c, -\frac{c}{a}, -\frac{c}{a} \right)^T \\ \mathbf{x}_+^* &\approx \left( 0^+, 0^+, 0^+ \right)^T = \mathbf{0}^+ \end{aligned} \right\} \text{for } c \rightarrow \infty \quad (10)$$

and

$$\left. \begin{aligned} \mathbf{x}_-^* &\approx \left( -c, -\frac{c}{a}, -\frac{c}{a} \right)^T \\ \mathbf{x}_+^* &\approx \left( 0^-, 0^-, 0^- \right)^T = \mathbf{0}^- \end{aligned} \right\} \text{for } c \rightarrow -\infty. \quad (11)$$

### III. CONSTRUCTED PERIODIC MOTIONS

For the Rössler system in Eq. (1), suppose there exists a periodic motion of  $\mathbf{x}(t) = \mathbf{x}(t+T)$  with period  $T$ . Consider a time interval  $[t_0, t_0 + T]$  uniformly partitioned into  $N$ -time intervals of  $[t_{k-1}, t_k]$  ( $k = 1, \dots, N$ ) with a time step of  $h = t_k - t_{k-1}$ . Using a midpoint discretization scheme for  $t \in [t_{k-1}, t_k]$ , a discrete mapping for period- $m$  motion  $\mathbf{x}^{(m)}(t)$  is developed as

$$P_k : \mathbf{x}_{k-1}^{(m)} \rightarrow \mathbf{x}_k^{(m)} \Rightarrow \mathbf{x}_k^{(m)} = P_k \mathbf{x}_{k-1}^{(m)}, \quad (12)$$

where  $\mathbf{x}_k^{(m)} = \mathbf{x}^{(m)}(t_k)$ . The implicit algebraic equation for the discrete mapping is given as

$$\mathbf{g}_k(\mathbf{x}_{k-1}^{(m)}, \mathbf{x}_k^{(m)}; h) = \mathbf{0}, \quad (13)$$

with

$$g_{k1} = x_k^{(m)} - x_{k-1}^{(m)} + \frac{1}{2}h \left( y_k^{(m)} + y_{k-1}^{(m)} + z_k^{(m)} + z_{k-1}^{(m)} \right),$$

$$g_{k2} = y_k^{(m)} - y_{k-1}^{(m)} - \frac{1}{2}h \left[ \left( x_k^{(m)} + x_{k-1}^{(m)} \right) + a \left( y_k^{(m)} + y_{k-1}^{(m)} \right) \right], \quad (14)$$

$$g_{k3} = z_k^{(m)} - z_{k-1}^{(m)} - \frac{1}{4}h \left[ 4b + \left( z_k^{(m)} + z_{k-1}^{(m)} \right) \left( x_k^{(m)} + x_{k-1}^{(m)} - 2c \right) \right].$$

Thus, such a mapping is called an implicit mapping. As in Luo,<sup>23,24</sup> such a discrete scheme has an accuracy of  $O(h^3)$ . Thus,  $h < 10^{-3}$  should be required for the accuracy of  $\varepsilon = 10^{-9}$  for each mapping. The resultant mapping of a period- $m$  motion is constructed by

$$P = \underbrace{P_{mN} \circ P_{mN-1} \circ \dots \circ P_1}_{mN\text{-actions}} : \mathbf{x}_0 \rightarrow \mathbf{x}_{mN}. \quad (15)$$

Thus,

$$\mathbf{x}_N^{(m)} = P\mathbf{x}_0 = P_{mN} \circ P_{mN-1} \circ \dots \circ P_1 \mathbf{x}_0, \quad (16)$$

with the  $mN$ -implicit algebraic equations as

$$\mathbf{g}_k(\mathbf{x}_{k-1}^{(m)}, \mathbf{x}_k^{(m)}; h) = \mathbf{0} \text{ for } k = 1, 2, \dots, mN, \quad (17)$$

and the periodicity condition is

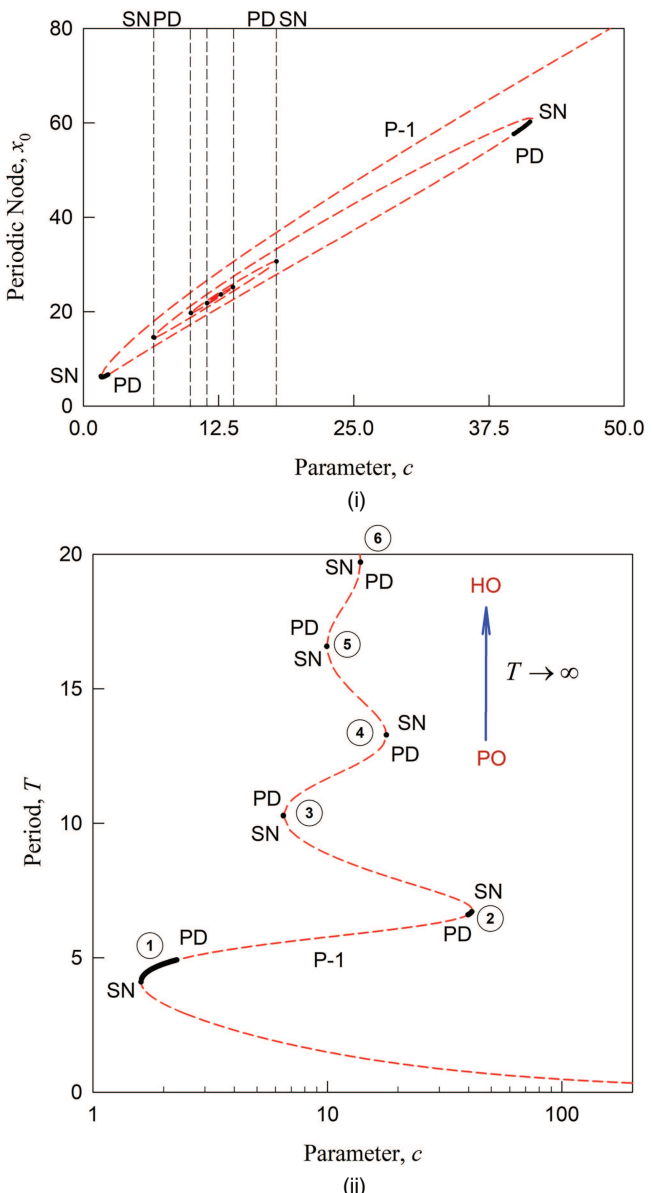


**FIG. 1.** Bifurcation tree varying with parameter  $c$  for an initial point on the Poincaré section: (i) initial point  $x_0$  and (ii) period  $T$ . Black solid curve: stable motion; red dashed curve: unstable motion. HO, homoclinic orbit; PD, period-doubling bifurcation; SN, saddle-node bifurcation; A, asymmetric motions; S, symmetric motions ( $a = 0.35$ ,  $b = 0.06$ ).

$$\mathbf{x}_0^{(m)} = \mathbf{x}_{mN}^{(m)}, \quad (18)$$

with the initial conditions on the selected Poincaré section of

$$y_0^{(m)} + z_0^{(m)} = 0. \quad (19)$$

**TABLE I.** Critical parameters of bifurcations of periodic motions ( $a = 0.35$ ,  $b = 0.06$ ,  $N = 1024$ ).  $c_{cr} \rightarrow \infty$  is from a Hopf bifurcation of the equilibrium  $\mathbf{x}^*$ , generating a period-1 motion with ( $T \rightarrow 0$ ). The corresponding equilibrium  $\mathbf{x}_+^* = \mathbf{0}^+$  is a (2:1)-saddle (two stable and one unstable). The layer “L0” will not have period-1 motion that goes to a homoclinic orbit. SN, saddle-node bifurcation; PD, period-doubling bifurcation.

Bifurcation	Layer	Critical parameter $c_{cr}$	Motion switching	
SN	L0	1.6021 $\leftarrow \infty$	P-1 motion layer switching	
	L1	1.6021 $\rightarrow$ 41.524 96		
	L2	6.476 89 $\leftarrow$ 41.524 96		
	L3	6.476 89 $\rightarrow$ 17.843 488 8		
	L4	9.934 915 08 $\leftarrow$ 17.843 488 8		
	L5	9.934 915 08 $\rightarrow$ 13.825 705 5		
	L6	11.420 385 3 $\leftarrow$ 13.825 705 5		
⋮				
PD	L1	2.2818 $\rightarrow$ 39.302 62	P-1 to P-2 motion	
	L3	6.545 15 $\rightarrow$ 17.809 74		
	L5	9.938 37 $\rightarrow$ 13.824 87		
	L7	11.420 480 2 $\rightarrow$ N/A		
	⋮			
	⋮			

The approximated discrete nodes  $\mathbf{x}_k^{(m)*}$  ( $k = 0, 1, \dots, mN$ ) in Eqs. (17)–(19) are solved by the Newton–Raphson method. For  $m = 1$ , the period-1 motion is obtained.

To determine the stability of periodic motions, the Jacobian matrix of the resultant mapping from Eq. (15) is

$$DP = \begin{bmatrix} \frac{\partial \mathbf{x}_N^{(m)}}{\partial \mathbf{x}_0^{(m)}} \end{bmatrix}_{(\mathbf{x}_0^{(m)*}, \mathbf{x}_1^{(m)*}, \dots, \mathbf{x}_N^{(m)*})} = DP_m DP_{mN-1} \cdots DP_1, \quad (20)$$

where

$$DP_k = \begin{bmatrix} \frac{\partial \mathbf{x}_k^{(m)}}{\partial \mathbf{x}_{k-1}^{(m)}} \end{bmatrix} = - \begin{bmatrix} \frac{\partial \mathbf{g}_k}{\partial \mathbf{x}_k^{(m)}} \end{bmatrix}^{-1} \begin{bmatrix} \frac{\partial \mathbf{g}_k}{\partial \mathbf{x}_{k-1}^{(m)}} \end{bmatrix}. \quad (21)$$

and the partial derivatives of  $\mathbf{g}_k$  from Eq. (17) are given by

$$\frac{\partial \mathbf{g}_k}{\partial \mathbf{x}_{k-1}} = \begin{bmatrix} -1 & \frac{1}{2}h & \frac{1}{2}h \\ -\frac{1}{2}h & -1 - \frac{1}{2}ah & 0 \\ -\frac{1}{4}h(z_k + z_{k-1}) & 0 & -1 - \frac{1}{4}h(x_k + x_{k-1} - 2c) \end{bmatrix}, \quad (22)$$

$$\frac{\partial \mathbf{g}_k}{\partial \mathbf{x}_k} = \begin{bmatrix} 1 & \frac{1}{2}h & \frac{1}{2}h \\ -\frac{1}{2}h & 1 - \frac{1}{2}ah & 0 \\ -\frac{1}{4}h(z_k + z_{k-1}) & 0 & 1 - \frac{1}{4}h(x_k + x_{k-1} - 2c) \end{bmatrix}, \quad (23)$$

$$\frac{\partial \mathbf{g}_k}{\partial h} = \frac{1}{4} \begin{bmatrix} 2(y_k + y + z_k + z_{k-1}) \\ -2[(x_k + x_{k-1}) + a(y_k + y_{k-1})] \\ -4b - (z_k + z_{k-1})(x_k + x_{k-1} - 2c) \end{bmatrix}. \quad (24)$$

The stability of the period- $m$  motion is determined through eigenvalue analysis. That is,

$$|DP - \lambda \mathbf{I}| = 0. \quad (25)$$

- (i) The period-1 solution is stable if all eigenvalues of  $DP(\lambda_{1,2,3})$  are within the unit circle.
- (ii) The period-1 solution is unstable if at least one eigenvalue of  $DP(\lambda_{1,2,3})$  is outside of the unit circle.

The bifurcation of periodic motions occurs when one eigenvalue or a pair of complex eigenvalues are on the unit circle.

- (i) If  $\lambda_i = 1$  with  $|\lambda_j| < 1$  ( $i, j \in \{1, 2\}; i \neq j$ ), the saddle-node bifurcation (SN) occurs.
- (ii) If  $\lambda_i = -1$  with  $|\lambda_j| < 1$  ( $i, j \in \{1, 2\}; i \neq j$ ), the period-doubling bifurcation (PD) occurs.
- (iii) If  $|\lambda_{i,j}| = 1$  with  $|\lambda_l| < 1$  ( $\lambda_i = \bar{\lambda}_j, l \neq i, j$ ), the Neimark bifurcation (NB) occurs.

The  $DP$  matrix contains a trivial eigenvalue of  $\lambda = 1$  for the autonomous system, which should be dropped.

#### IV. PERIODIC MOTIONS TO HOMOCLINIC ORBITS

Using the discrete mapping method, the analytical prediction of periodic motions in the Rössler system will be carried out with a prescribed accuracy. The discrete mapping in Eq. (4) has a computational accuracy of  $\varepsilon = O(h^3) = 10^{-9}$ . A time step of  $h < 5 \times 10^{-3}$  is required for such accuracy through the node number  $N$  to control per period. Consider two system parameters of the Rössler system as

$$a = 0.35, b = 0.06. \quad (26)$$

From the above system parameter, the bifurcation tree of period-1 motions to the homoclinic orbit is developed, and the initial point  $x_0$  on the Poincaré section, varying with parameter  $c \in (0, 50)$ , is presented in Fig. 1. In Fig. 1(i), a bifurcation tree of period-1 motions to the homoclinic orbit for initial points on the Poincaré

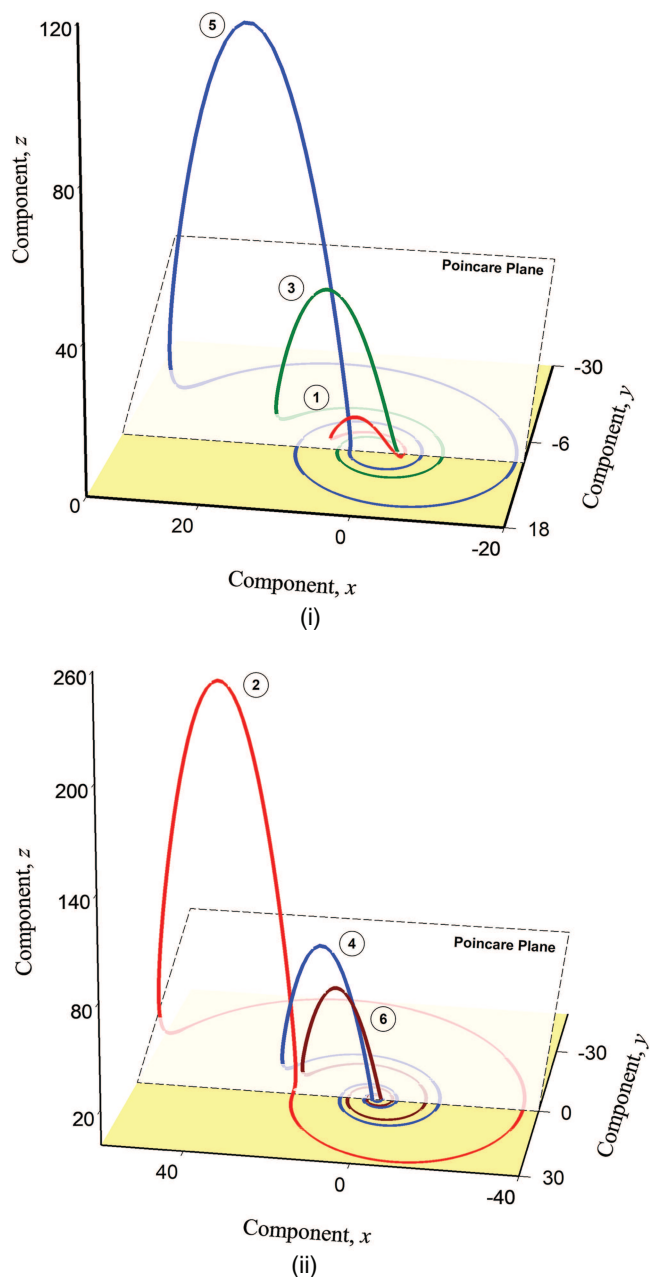


**FIG. 2.** Trajectories for periodic motions on the bifurcation tree: (i) stable period-1 motion on the left side of the bifurcation tree and (ii) stable period-1 motion on the right side of the bifurcation tree ( $a = 0.35$ ,  $b = 0.06$ ).

section is presented. The period-1 motion starts from a saddle-node bifurcation at  $c_{cr} \approx \infty$ , which is the Hopf bifurcation of the equilibrium. Such a starting periodic motion has a period of  $T \rightarrow 0$  and large rotation speed near  $\mathbf{x}_-^* \approx (-c, -\frac{c}{a}, -\frac{c}{a})^T$ .

With decreasing parameter  $c$ , such an unstable period-1 motion with at least one eigenvalue greater than  $+1$  arrives to another saddle-node bifurcation with an eigenvalue of  $\lambda = +1$ . The period-1 motion returns and becomes stable. With increasing parameter  $c$ , the period-1 motion has a period-doubling bifurcation, and period-1 motion becomes unstable with at least negative eigenvalue less than  $-1$ . After period-doubling, the period-2 motion will appear, which will not be presented herein and will be discussed in sequel. Such an unstable period-1 motion arrives to another period-doubling bifurcation. The period-1 motion becomes stable and continues to a saddle-node bifurcation. The period-1 motion will counterclockwise turn back. Continuously, the period-1 motions will move to another saddle-node bifurcation with decreasing parameter  $c$ . Such a counterclockwise spiraling movement of the bifurcation tree will arrive to the homoclinic orbit. The period of period-1 motion is computed by  $T = N \times h$ . For the homoclinic orbit, the period of periodic motion should be infinite. For such a bifurcation tree of period-1 motion to a homoclinic orbit, the period for such a bifurcation tree is presented in Fig. 1(ii). The labeled numbers are for simulations of period-1 motions: the left and right stable periodic motions of the bifurcation tree. Once the period  $T$  becomes infinitely large, the homoclinic orbit is obtained. From the bifurcation tree, there are different layers of periodic motion with and without period-doubling bifurcations. The critical values for saddle-node and period-doubling bifurcations for period-1 motions are listed in Table I.

For comparison, similar period-1 motions are placed in the same figure. For instance, stable period-1 motions on the left and right sides of the bifurcation tree are presented for  $a = 0.35$  and  $b = 0.06$  in Figs. 2(i) and 2(ii), respectively. The initial conditions are listed in Table II. The chosen values for parameter  $c$  are tabulated. The circled numbers are from the bifurcation tree for the right and left side of the bifurcation tree of period-1 motions. In Fig. 2(i), three period-1 motions that are on the left side of the bifurcation tree are presented. For the periodic motions (No. 1., No. 3, and No. 5), the slow movement has no cycle, 1.5 cycles, and 2 cycles. In Fig. 2(ii), three period-1 motions that are on the right side of the bifurcation tree are presented. For the periodic motions (No. 2., No. 4, No. 6), the slow movement has about 0.5, 2.5, and 3 cycles. The fast movements for three period-1 motions become large with increasing parameter  $c$ .

## V. A BI-PARAMETER ORIGAMI STRUCTURE OF PERIODIC MOTIONS

To determine a system parameter for the critical point of periodic motions, such a system parameter is considered an unknown variable for a specific eigenvalue  $\lambda_i$ , which is determined by

$$(DP - \lambda_i \mathbf{I}) \mathbf{v}^{(i)} = \mathbf{0},$$

$$\sum_{s=1}^3 (\nu_s^{(i)})^2 = 1, \quad (27)$$

with  $\mathbf{v}^{(i)} = (\nu_1^{(i)}, \nu_2^{(i)}, \nu_3^{(i)})^T$ ,

**TABLE II.** Initial conditions and parameter  $c$  of numerical simulations ( $a = 0.35$ ,  $b = 0.06$ ).

	Number	Parameter $c$	Initial conditions
Figure 2(i)	1	2.1	(6.424 854, -1.471 657, 1.471 656)
	3	6.476 895 7	(14.559 265, -4.388 423, 4.388 423)
	5	9.934 916 5	(19.688 519, -6.014 809, 6.014 809)
Figure 2(ii)	2	40.8	(59.284 701, -18.173 644, 18.173 643)
	4	17.843 488 6	(30.648 243, -9.676 526, 9.676 526)
	6	13.825 704	(25.169 852, -7.822 456, 7.822 456)

with the corresponding periodic motion determined by

$$\begin{aligned} \mathbf{g}_k(\mathbf{x}_{k-1}^{(m)}, \mathbf{x}_k^{(m)}, h) &= \mathbf{0} \quad (k = 1, 2, \dots, mN), \\ \mathbf{x}_0^{(m)} &= \mathbf{x}_{mN}^{(m)}, \\ y_0^{(m)} + z_0^{(m)} &= 0. \end{aligned} \quad (28)$$

From the above equations in Eqs. (27) and (28), the parameter, periodic solution and eigenvectors are computed. To solve the above equations, the corresponding Jacobian matrix for the

Newton–Raphson method needs the following derivatives for  $DP$ :

$$\frac{\partial DP}{\partial \mathbf{x}_k} = \sum_{j=k}^{k+1} \underbrace{DP_{mN} DP_{mN-1} \dots DP_{j+1}}_{(mN-j) \text{ actions}} \underbrace{\frac{\partial DP_j}{\partial \mathbf{x}_k} \underbrace{DP_{j-1} DP_{k-2} \dots DP_1}_{(j-1) \text{ actions}}}_{}, \quad (29)$$

where

$$\frac{\partial DP_k}{\partial \mathbf{x}_k} = -\left(\frac{\partial \mathbf{g}_k}{\partial \mathbf{x}_k}\right)^{-1} \left[ \frac{\partial^2 \mathbf{g}_k}{\partial \mathbf{x}_k^2} \left(\frac{\partial \mathbf{g}_k}{\partial \mathbf{x}_k}\right)^{-1} \frac{\partial \mathbf{g}_k}{\partial \mathbf{x}_{k-1}} + \frac{\partial^2 \mathbf{g}_k}{\partial \mathbf{x}_k \partial \mathbf{x}_{k-1}} \right], \quad (30)$$

$$\frac{\partial DP_k}{\partial \mathbf{x}_{k-1}} = -\left(\frac{\partial \mathbf{g}_k}{\partial \mathbf{x}_k}\right)^{-1} \left[ \frac{\partial^2 \mathbf{g}_k}{\partial \mathbf{x}_{k-1} \partial \mathbf{x}_k} \left(\frac{\partial \mathbf{g}_k}{\partial \mathbf{x}_k}\right)^{-1} \frac{\partial \mathbf{g}_k}{\partial \mathbf{x}_{k-1}} + \frac{\partial^2 \mathbf{g}_k}{\partial \mathbf{x}_{k-1}^2} \right], \quad (31)$$

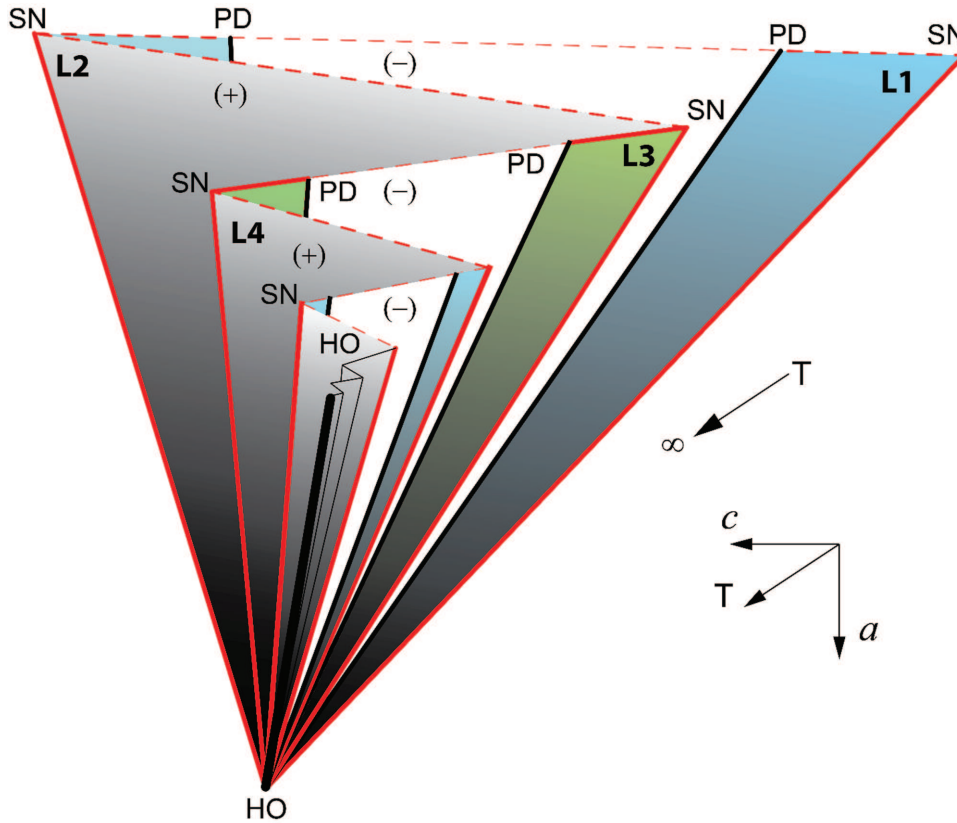


**FIG. 3.** The origami structure of periodic motions to homoclinic orbits in the Rössler system. The layer section area shrinks to the homoclinic orbit (HO). On the period-doubling layer: the shaded area for a stable region; the white area for an unstable region with a negative eigenvalue (−). On the no period-doubling layer: the gradient area for unstable motion with a positive eigenvalue (+). The edge lines are for a saddle-node (SN), and the black solid lines are for period-doubling bifurcation. All such curves approaching the homoclinic orbit (HO) at the pivot point. One of the eigenvalues of  $DP$  approaches positive or negative infinity near homoclinic orbits. The periods of periodic motions approach infinity.

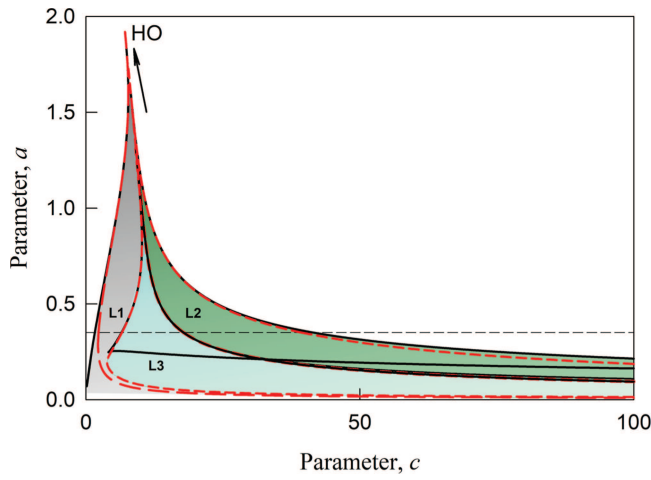


**FIG. 4.** Parameter maps of  $(c, a)$  ( $b = 0.06$ ) for period-1 motions on the different layers for overlap for three layers. The saddle-node bifurcations (SN) are black solid curves. The period-doubling bifurcations (PD) are blue dashed curves. The equi-eigenvalue curves are red dashed curves. HO: homoclinic orbits.

and

$$\frac{\partial^2 \mathbf{g}_k}{\partial \mathbf{x}_{k-1}^2} = \frac{\partial^2 \mathbf{g}_k}{\partial \mathbf{x}_{k-1} \partial \mathbf{x}_k} = \begin{bmatrix} 0 & 0 & 0 & 0 & 0 & 0 & 0 & 0 \\ 0 & 0 & 0 & 0 & 0 & 0 & 0 & 0 \\ 0 & 0 & -\frac{1}{2}h & 0 & 0 & 0 & -\frac{1}{2}h & 0 \end{bmatrix}, \quad (32)$$

$$\begin{aligned} \frac{\partial}{\partial h} \frac{\partial \mathbf{g}_k}{\partial \mathbf{x}_k} &= \frac{\partial}{\partial h} \frac{\partial \mathbf{g}_k}{\partial \mathbf{x}_{k-1}} \\ &= \begin{bmatrix} 0 & \frac{1}{2} & \frac{1}{2} \\ -\frac{1}{2} & -\frac{1}{2}\beta_1 & 0 \\ -\frac{1}{4}(z_k + z_{k-1}) & 0 & -\frac{1}{4}(x_k + x_{k-1} - 2r) \end{bmatrix}. \end{aligned} \quad (33)$$

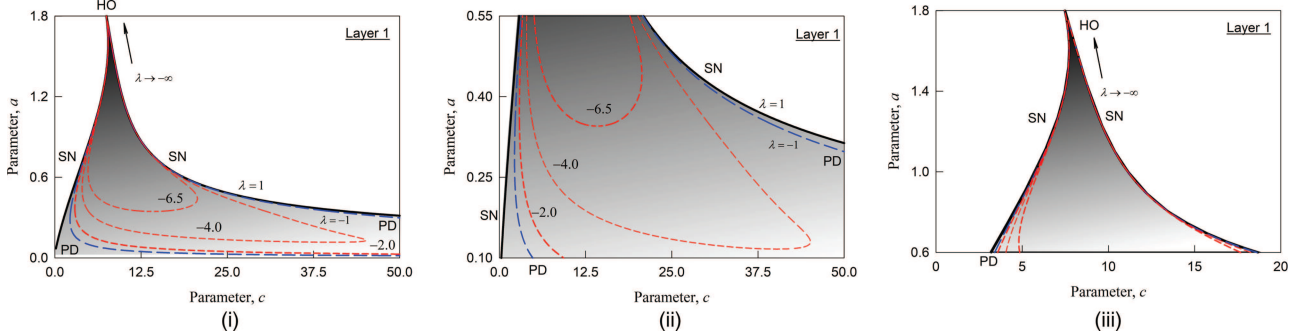


**FIG. 5.** Parameter maps of  $(c, a)$  ( $b = 0.06$ ) for period-1 motions on the different layers for first layer with period-doubling bifurcations: (i) global view, (ii) bottom zoom, (iii) top zoom. The saddle-node bifurcations (SN) are black solid curves. The period-doubling bifurcations (PD) are blue dashed curves. The equi-eigenvalue curves are red dashed curves. HO: homoclinic orbits.

If a system parameter  $a$  is considered a variable,

$$\frac{\partial}{\partial a} \frac{\partial \mathbf{g}_k}{\partial \mathbf{x}_k} = \frac{\partial}{\partial a} \frac{\partial \mathbf{g}_k}{\partial \mathbf{x}_{k-1}} = \text{diag}(0, -h/2, 0). \quad (34)$$

If a system parameter  $c$  is considered a variable,

$$\frac{\partial}{\partial c} \frac{\partial \mathbf{g}_k}{\partial \mathbf{x}_k} = \frac{\partial}{\partial c} \frac{\partial \mathbf{g}_k}{\partial \mathbf{x}_{k-1}} = \text{diag}(0, 0, h/2). \quad (35)$$

For the saddle-node bifurcation of  $\lambda_i = +1$ , the following equations are used:

$$\begin{aligned} (DP - (+1)\mathbf{I})\mathbf{v}^{(SN)} &= \mathbf{0}, \\ \sum_{s=1}^3 (\mathbf{v}_s^{(SN)})^2 &= 1, \\ \text{with } \mathbf{v}^{(SN)} &= \left( v_1^{(SN)}, v_2^{(SN)}, v_3^{(SN)} \right)^T, \\ \mathbf{g}_k(\mathbf{x}_{k-1}^{(m)}, \mathbf{x}_k^{(m)}, h) &= \mathbf{0} \quad (k = 1, 2, \dots, mN), \\ \mathbf{x}_0^{(m)} &= \mathbf{x}_{mN}^{(m)}, \\ y_0^{(m)} + z_0^{(m)} &= 0. \end{aligned} \quad (36)$$

For the period-doubling bifurcation of  $\lambda_i = -1$ , the following equations are used:

$$\begin{aligned} (DP - (-1)\mathbf{I})\mathbf{v}^{(PD)} &= \mathbf{0}, \\ \sum_{s=1}^3 (\mathbf{v}_s^{(PD)})^2 &= 1, \\ \text{with } \mathbf{v}^{(PD)} &= \left( v_1^{(PD)}, v_2^{(PD)}, v_3^{(PD)} \right)^T, \\ \mathbf{g}_k(\mathbf{x}_{k-1}^{(m)}, \mathbf{x}_k^{(m)}, h) &= \mathbf{0} \quad (k = 1, 2, \dots, mN), \\ \mathbf{x}_0^{(m)} &= \mathbf{x}_{mN}^{(m)}, \\ y_0^{(m)} + z_0^{(m)} &= 0. \end{aligned} \quad (37)$$

From the bifurcation tree of period-1 motion to the homoclinic orbit, the origami structure of periodic motions to homoclinic orbits in the bi-parameter space is sketched in Fig. 3. The Hopf

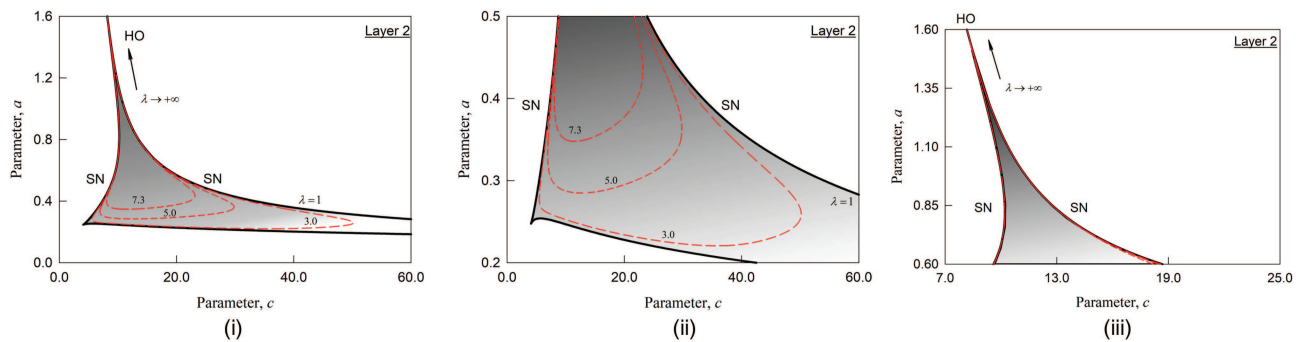


**FIG. 6.** Parameter maps of  $(c, a)$  ( $b = 0.06$ ) for period-1 motions on the different layers for the second layer without period-doubling bifurcations: (i) global view, (ii) bottom zoom, (iii) top zoom. The saddle-node bifurcations (SN) are black solid curves. The period-doubling bifurcations (PD) are blue dashed curves. The equi-eigenvalue curves are red dashed curves. HO: homoclinic orbits.

bifurcation of the equilibrium at  $x^*$  with  $c \rightarrow 0$  generates a new unstable period-1 motion with a period of  $T \rightarrow 0$ . Such a point can be called the birth of period-1 motions from such an equilibrium. Thus, with decreasing parameter  $c$ , the period of such a periodic motion will increase until the first saddle-node bifurcation of the period-1 motion occurs. On such a layer of period-1 motion (L0), the period-1 motion is from the starting saddle-node period-1 motion to the saddle-node period-1 motion of the first layer. On the layer (L0), period-1 motion will not go to the homoclinic orbit. Thus, the origami structure will start from the first layer to the homoclinic orbits with infinite layers, as presented in Fig. 3. On the period-doubling layer, two shaded areas are for stable period-1 motions. The white area is for unstable period-1 motion with a negative eigenvalue (−). On the no period-doubling layer, the gradient shaded area is for unstable motion with a positive eigenvalue (+). The edge lines are for saddle-node (SN), and the black solid lines are for period-doubling bifurcations. All such

curves approach the homoclinic orbit (HO) at the pivot point. One of the eigenvalues of  $DP$  approaches positive or negative infinity near homoclinic orbits. The periods of periodic motions approach infinity.

From the origami structure, for each layer, the saddle-node bifurcation curves and period-doubling bifurcation curves are developed in the parameter space of  $(c, a)$  from Eqs. (36) and (37), respectively. In addition, the equi-eigenvalue curves are presented from Eqs. (27) and (28). For period-1 motions with positive eigenvalues, the maximum equi-eigenvalue curves of period-1 motions are presented. For periodic motions with negative eigenvalues, the minimum equi-eigenvalue curves of period-1 motions are presented. Once the maximum or minimum equi-eigenvalue curves goes to positive or negative infinity on each layer, the homoclinic orbits based on the positive and negative eigenvalues are obtained. The parameter maps in the  $(c, a)$ -space is presented for  $b = 0.06$  in Figs. 4–7.

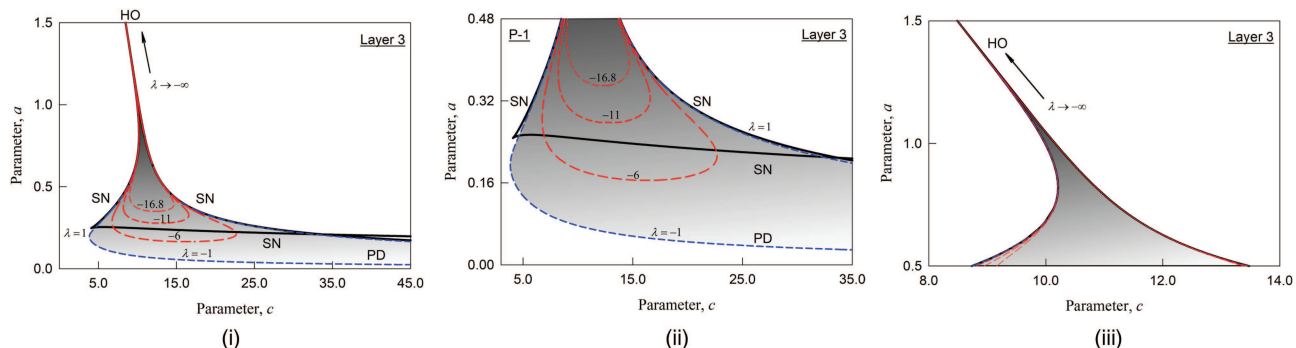


**FIG. 7.** Parameter maps of  $(c, a)$  ( $b = 0.06$ ) for period-1 motions on the different layers for the third layer with period-doubling bifurcations: (i) global view, (ii) bottom zoom, (iii) top zoom. The saddle-node bifurcations (SN) are black solid curves. The period-doubling bifurcations (PD) are blue dashed curves. The equi-eigenvalue curves are red dashed curves. HO: homoclinic orbits.

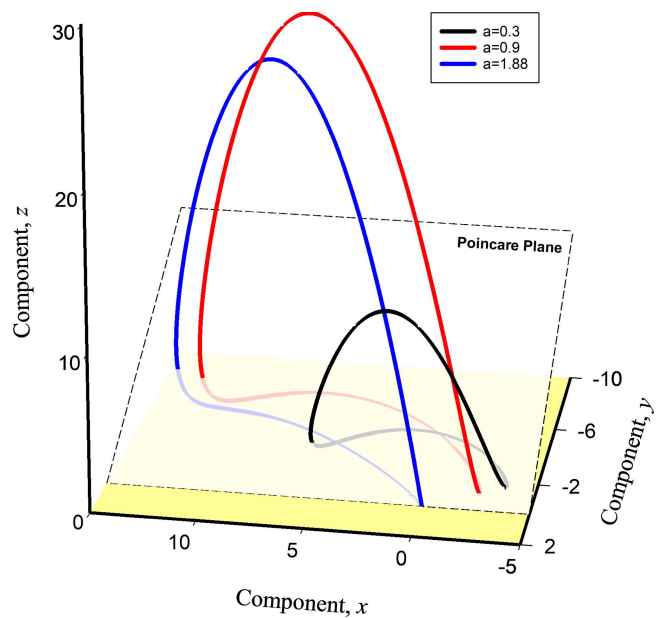


**FIG. 8.** The 3D view of the trajectories for periodic orbits to the approximate homoclinic orbit ( $b = 0.06$ ) based on the system parameters  $(c, a) = (1.307628, 0.3)$ ,  $(5.168186, 0.9)$ , and  $(7.657304, 1.899)$  on the first layer of the bi-parameter origami structure. The approximate homoclinic orbit passes through the equilibrium point.

In Fig. 4, the global view of the parameter map with multiple layers is presented. Different layers are depicted through different colors. The highest tip is close to the homoclinic orbits. To clearly observe the bifurcation curves on the parameter maps, the parameter map of  $(c, a)$  for the first layer with period-doubling bifurcations is presented in Figs. 5(i)–5(iii). In Fig. 5(i), the global view of the parameter map for period-1 motion with period-doubling is presented. The saddle-node bifurcations with  $\lambda = 1$  are two boundaries of the parameter map, and period-doubling curves are depicted through dashed blue curves, which are also labeled with  $\lambda = -1$ . The minimum equi-eigenvalue curves are depicted through dashed red curves. It is clearly observed that negative equi-eigenvalues decrease with a direction to the homoclinic orbit. For clear views, the bottom and top views of the global parameter map for the first layer are zoomed in Figs. 5(ii) and 5(iii). The equi-eigenvalue curves are clearly presented. The parameter map of  $(c, a)$  for the second layer without period-doubling bifurcations is presented in Figs. 6(i)–6(iii). The global view of the parameter map for period-1

motion is presented in Fig. 6(i). The saddle-node bifurcations with  $\lambda = 1$  are two boundaries of the parameter map. The positive equi-eigenvalue increases with a direction to the homoclinic orbit. The bottom and top views of the global parameter map for the second layer are zoomed in Figs. 6(ii) and 6(iii). Similarly, the parameter map of  $(c, a)$  for the third layer with period-doubling bifurcations is presented in Figs. 7(i)–7(iii). In Fig. 7(i), the global view of the parameter map for period-1 motion with period-doubling is presented. The period-doubling boundary is partially out of the boundaries of the saddle-node bifurcation. The three saddle-node bifurcation boundaries exist. The minimum equi-eigenvalue curves are also depicted through dashed red curves. The negative equi-eigenvalues decrease with a direction to the homoclinic orbit. The bottom and top views of the global parameter map for the first layer are zoomed in Figs. 7(ii) and 7(iii). In a similar fashion, one can develop other parameter maps for others layers until the homoclinic orbits.

## VI. HOMOCLINIC ORBITS ON SPECIFIC LAYERS

From the analytical prediction, periodic orbits and approximated homoclinic orbits in the Rössler system can be obtained from different layers on the origami structure. From the parameter space, periodic orbits to the corresponding approximate homoclinic orbits are to be presented herein. In the following plots, the initial conditions are selected on the Poincaré plane of  $y + z = 0$ .

In Fig. 8, the 3D view of the trajectories of period-1 motions to the approximate homoclinic orbits are presented with  $b = 0.06$  for  $(c, a) = (1.307628, 0.3)$ ,  $(5.168186, 0.9)$ , and  $(7.657304, 1.899)$ , respectively. The corresponding initial conditions are listed in Table III. The trajectory of period-1 motions for  $(c, a) = (1.307628, 0.3)$  is very small, which is far away from the homoclinic orbit. With increasing parameter  $a$ , the periodic motion will approach the homoclinic orbit for  $(c, a) = (5.168186, 0.9)$ . The trajectory of such periodic motions becomes large. With further increasing parameter  $a$ , the approximate homoclinic orbit with the saddle equilibrium is presented for  $(c, a) = (7.657304, 1.899)$ . Such an approximate homoclinic orbit with a negative eigenvalue is clearly observed.

In Fig. 9, the 3D view of the trajectories of period-1 motions to the approximate homoclinic orbits are presented with  $b = 0.06$  for  $(c, a) = (23.859380, 0.5)$ ,  $(11.133112, 1.0)$ , and  $(8.515895, 1.5)$  on the second layer, and the corresponding initial conditions are listed in Table IV. Compared to the other trajectories, as in Fig. 9(i), the trajectory of the period-1 motion for  $(c, a) = (23.859380, 0.5)$  is very large because  $c = 23.859380$  is large. In addition, the trajectory is far away from the homoclinic orbit. To clearly view the

**TABLE III.** Initial conditions of numerical simulations ( $b = 0.06$ ) on the first layer.

Parameter $a$	Parameter $c$	Initial conditions	Types
0.3	1.307 628	(5.733 600, -1.846 462, 1.846 462)	Period-1 PO
0.9	5.168 186	(11.712 978, -3.805 303, 3.805 303)	Period-1 PO
1.88	7.657 304	(13.037 757, -4.050 959, 4.050 959)	Period-1 HO

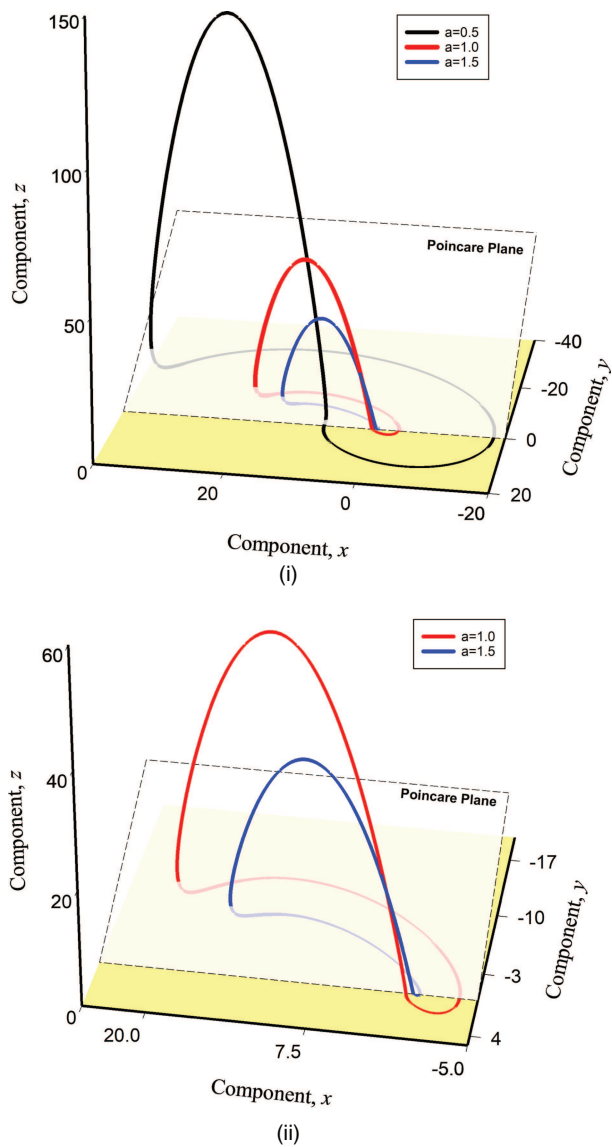


**FIG. 9.** The 3D view of the trajectories for periodic orbits to the approximate homoclinic orbit ( $b = 0.06$ ) based on the system parameters  $(c, a) = (23.859380, 0.5)$ ,  $(11.133112, 1.0)$ , and  $(7.657304, 1.899)$  on the second layer of the bi-parameter origami structure: (i) the global view and (ii) the zoomed view. The approximate homoclinic orbit passes through the equilibrium point.

**TABLE IV.** Initial conditions of numerical simulations ( $b = 0.06$ ) on the second layer.

Parameter $a$	Parameter $c$	Initial conditions	Types
0.5	23.859 380	$(38.179\ 980, -12.123\ 795, 12.123\ 795)$	Period-1 PO
1.0	11.133 112	$(20.167\ 777, -6.240\ 415, 6.240\ 415)$	Period-1 PO
1.5	8.515 895	$(15.568\ 467, -4.851\ 708, 4.851\ 708)$	Period-1 HO

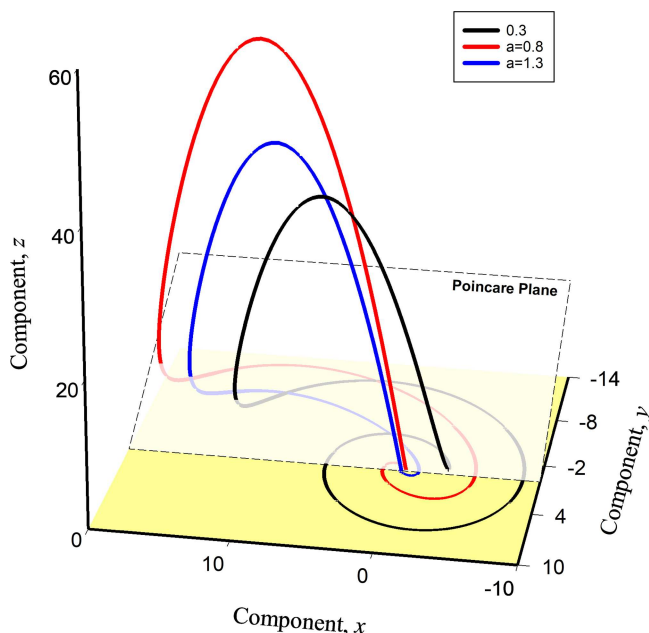


**FIG. 10.** The 3D view of the trajectories for periodic orbits to the approximate homoclinic orbit ( $b = 0.06$ ) based on the system parameters  $(c, a) = (5.454908, 0.3)$ ,  $(10.203527, 0.8)$ , and  $(9.136153, 1.3)$  on the third layer of the bi-parameter origami structure. The approximate homoclinic orbit passes through the equilibrium point.

homoclinic orbit, the zoomed view is given in Fig. 9(ii). The largest periodic orbit is removed from the zoomed view. The trajectory of the period-1 motion for  $(c, a) = (11.133112, 1.0)$  is almost close to the homoclinic orbit. With increasing parameter  $a$ , the trajectory of the approximate homoclinic orbit for  $(c, a) = (8.515895, 1.5)$  is obtained with the saddle equilibrium.

In Fig. 10, the 3D view of the trajectories of period-1 motions to the approximate homoclinic orbit is presented for  $(c, a) = (5.454908, 0.3)$ ,  $(10.203527, 0.8)$ , and  $(9.136153, 1.3)$  on the third layer, and the initial conditions are listed in Table V. The trajectory of period-1 motions for  $(c, a) = (5.454908, 0.3)$  is far away from the homoclinic orbit. With increasing parameter  $a$ , the periodic motion for  $(c, a) = (10.203527, 0.8)$  is almost close to the homoclinic orbit. With further increasing parameter  $a$ , the approximate homoclinic orbit with the saddle equilibrium is obtained for  $(c, a) = (9.136153, 1.3)$ . Such an approximate homoclinic orbit has negative eigenvalues.

**TABLE V.** Initial conditions of numerical simulations ( $b = 0.06$ ) on the third layer.

Parameter $a$	Parameter $c$	Initial conditions	Types
0.3	5.454 908	(13.031 081, -3.881 428, 3.881 428)	Period-1 PO
0.8	10.203 527	(19.262 827, -5.990 117, 5.990 117)	Period-1 PO
1.3	9.136 153	(16.812 017, -5.240 486, 5.240 486)	Period-1 HO

## VII. CONCLUSIONS

In this paper, the origami structure of period-1 motions to spiral homoclinic orbits in parameter space was developed for the Rössler system. Such an origami structure will guide one to find possible periodic orbits and corresponding homoclinic orbits in the Rössler system. The origami structure has two edges of each layer, formed by the saddle-node bifurcations. For the period-1 motion origami structure, there are two types of layers *with* and *without* a pair of period-doubling bifurcations. In addition, a method for how to construct the parameter map was presented, and the equi-eigenvalue curves in the parameter map were developed for each layer. Such a method is much accurate and better than the Lyapunov exponent method. The equi-eigenvalue curves are accurate and global rather than the local and numerically averaging values in the Lyapunov exponent method. The method for such equi-eigenvalues can directly detect the behaviors of periodic orbits in parameter maps. To verify the mentioned methods, the origami structures of period-1 motion to homoclinic orbits for the Rössler were developed, and such a study provides the mathematical mechanisms of period-1 motions to the homoclinic orbits in the Rössler system. The infinitely many homoclinic orbits are induced through unstable periodic motions with positive and negative eigenvalues.

## AUTHOR DECLARATIONS

### Conflict of Interest

The authors have no conflicts to disclose.

### Author Contributions

**Siyuan Xing:** Conceptualization (equal); Methodology (equal); Writing – original draft (equal); Writing – review & editing (equal). **Albert C. J. Luo:** Conceptualization (equal); Methodology (equal); Supervision (equal); Writing – original draft (equal); Writing – review & editing (equal).

## DATA AVAILABILITY

The data that support the findings of this study are available from the corresponding author upon reasonable request.

## REFERENCES

- <sup>1</sup>O. E. Rössler, “An equation for continuous chaos,” *Phys. Lett. A* **57**, 397–398 (1976).
- <sup>2</sup>O. E. Rössler, “Different types of chaos in two simple differential equations,” *Z. Nat. A* **31**, 1664–1670 (1976).
- <sup>3</sup>E. N. Lorenz, “Deterministic nonperiodic flow,” *J. At. Sci.* **20**(2), 130–141 (1963).
- <sup>4</sup>L. P. Shilnikov, “A case of the existence of denumerable set of periodic motions,” *Dokl. Akad. Nauk SSSR* **160**, 558–561 (1965).
- <sup>5</sup>L. P. Shilnikov, “On a Poincaré–Birkhoff problem,” *Mat. Sb.* **116**(3), 378–397 (1967).
- <sup>6</sup>N. K. Gavrilov and L. P. Shilnikov, “On three-dimensional dynamical systems close to systems with a structurally unstable homoclinic curve. I,” *Math. USSR-Sb.* **88**, 475–492 (1972).
- <sup>7</sup>N. K. Gavrilov and L. P. Shilnikov, “On three-dimensional dynamical systems close to systems with a structurally unstable homoclinic curve: II,” *Math. USSR-Sb.* **19**, 139–156 (1973).
- <sup>8</sup>S. Guo and A. C. J. Luo, “On infinite homoclinic orbits induced by unstable periodic orbits in the Lorenz system,” *Chaos* **31**, 043106 (2021).
- <sup>9</sup>S. Guo and A. C. J. Luo, “Bifurcation trees of (1:2)-asymmetric periodic motions with corresponding infinite homoclinic orbits in the Lorenz system,” *J. Vib. Test. Syst. Dyn.* **5**(4), 373–406 (2021).
- <sup>10</sup>S. Guo and A. C. J. Luo, “A family of periodic motions to chaos with infinite homoclinic orbits in the Lorenz system,” *Lobachevskii J. Math.* **42**(14), 3382–3437 (2021).
- <sup>11</sup>S. Y. Guo and A. C. J. Luo, “To infinitely many spiral homoclinic orbits from periodic motions in the Lorenz system,” *Int. J. Dyn. Control* (published online 2022).
- <sup>12</sup>A. Arneodo, P. Coullet, and C. Tresser, “Oscillators with chaotic behavior: An illustration of a theorem by Shilnikov,” *J. Stat. Phys.* **27**, 171–182 (1982).
- <sup>13</sup>P. Glendinning and C. Sparrow, “Local and global behavior near homoclinic orbits,” *J. Stat. Phys.* **35**, 645–696 (1984).
- <sup>14</sup>P. Gaspard, R. Kapral, and G. Nicolis, “Bifurcation phenomena near homoclinic systems: A two-parameter analysis,” *J. Stat. Phys.* **35**(5), 697–727 (1984).
- <sup>15</sup>L. Gardini, “Hopf bifurcations and period-doubling transitions in Rössler model,” *Nuovo Cimento B Ser.* **89**(2), 139–160 (1985).
- <sup>16</sup>A. Arneodo, P. H. Coullet, and C. Tresser, “Asymptotic chaos,” *Phys. D: Nonlinear Phenom.* **14**(3), 327–347 (1985).
- <sup>17</sup>A. R. Champneys and Y. A. Kuznetsov, “Numerical detection and continuation of codimension-two homoclinic bifurcations,” *Int. J. Bifurc. Chaos* **04**, 785–822 (1994).
- <sup>18</sup>C. Letellier, P. Dutertre, and B. Maheu, “Unstable periodic orbits and templates of the Rössler system: Toward a systematic topological characterization,” *Chaos* **5**, 271–282 (1995).
- <sup>19</sup>R. Barrio, F. Blesa, and S. Serrano, “Qualitative analysis of the Rössler equations: Bifurcations of limit cycles and chaotic attractors,” *Phys. D: Nonlinear Phenom.* **238**, 1087–1100 (2009).
- <sup>20</sup>R. Barrio, F. Blesa, A. Dena, and S. Serrano, “Qualitative and numerical analysis of the Rössler model: Bifurcations of equilibria,” *Comput. Mathematics Appl.* **62**, 4140–4150 (2011).
- <sup>21</sup>R. Barrio, F. Blesa, S. Serrano, T. Xing, and A. Shilnikov, “Homoclinic spirals, theory and numerics,” in *Progress and Challenges in Dynamical Systems* (Springer, Berlin, 2013).
- <sup>22</sup>S. Malykh, Y. Bakhanova, A. Kazakov, K. Pusuluri, and A. Shilnikov, “Homoclinic chaos in the Rössler system,” *Chaos* **30**, 113126 (2020).
- <sup>23</sup>A. C. J. Luo, *Discretization and Implicit Mapping Dynamics* (Springer, Berlin, 2015).
- <sup>24</sup>A. C. J. Luo, “Periodic flows to chaos based on discrete implicit mappings of continuous nonlinear systems,” *Int. J. Bifurc. Chaos* **25**(3), 1550044 (2015).
- <sup>25</sup>A. C. J. Luo and Y. Guo, “A semi-analytical prediction of periodic motions in Duffing oscillator through mapping structures,” *Discontinuity, Nonlinearity, Complexity* **4**(2), 121–150 (2015).
- <sup>26</sup>A. C. J. Luo and J. Huang, “Analytical solutions for asymmetric periodic motions to chaos in a hardening Duffing oscillator,” *Nonlinear Dyn.* **72**(1–2), 417–438 (2013).